European Congress on Computational Methods in Applied Sciences and Engineering
ECCOMAS 2004
P. Neittaanmäki, T. Rossi, S. Korotov, E. Oñate, J. Périaux, and D. Knörzer (eds.)
Jyväskylä, 24–28 July 2004

FULLY EXPLICIT AND SEMI-IMPLICIT CBS PROCEDURES FOR INCOMPRESSIBLE FLOWS

N. Massarotti*, F. Arpino*, P. Nithiarasu°

*Department of Mechanics, Structures and Environment (DiMSAT)
Via G. Di Biasio 43, 03043 Cassino, University of Cassino, Italy
e-mail: massarotti@unicas.it, f.arpino@unicas.it
and
° Civil and Computational Engineering
Singleton Park, SA2 8PP Swansea University of Wales Swansea, UK
e-mail: P.Nithiarasu@Swansea.ac.uk

Key words: CBS, incompressible flows, explicit, semi-implicit, heat transfer.

Abstract. *In this paper two different formulations of the Characteristic-Based-Split algorithm are used to solve incompressible flow with heat transfer. The first is based on the original semi-implicit version of the CBS, which was used in the early days of the scheme development. More recently a new, fully explicit version of the scheme, based on the concept of artificial compressibility, has been developed by the authors. In order to compare the two formulations, several benchmark solutions are presented, for both steady and unsteady flows.*

1 INTRODUCTION

An extensive study on fundamental fluid flow and heat transfer problems is very important in many engineering applications such as thermal insulation, cooling of electronic devices, solar energy, nuclear reactors, etc. The velocity and temperature fields are mathematically described using the Navier-Stokes equations and in many applications the flow can be considered incompressible. The numerical solution of incompressible Navier-Stokes equations has been studied extensively, and Finite Element solutions have been proposed since the early 1970s [1, 2, 3, 5]. The standard Galerkin method, being equivalent to a central difference approximation, produces spurious pressure solutions [5]. This problem is usually solved with a proper choice of the velocity and pressure approximations, or using some kind of stabilization technique, such as those inspired by the up-winding schemes developed originally for finite differences [6]. However, schemes such as the Taylor-Galerkin or the Characteristic Galerkin method have shown that balancing diffusion terms emerge naturally when the equations are discretized in time. In particular, in the Characteristic Galerkin method the temporal derivative is discretized along the characteristic, whereon which the equation is self-adjoint in nature and thus spatial Galerkin approximation is optimal. The Characteristic-Based-Split (CBS) ia a time iterative solution algorithm that has shown to be very general for the solution of the Navier-Stokes equations [5, 7]. For the solution of incompressible flows with the CBS, it was initially necessary to use a semi-implicit formulation, which suffers from some restrictions on the time step, and the necessity for time consuming solution to simultaneous equations. Recently, one of the authors of this work, presented a new version of the scheme for the solution of incompressible flows, based on the artificial compressibility concept [8]. The result is a fully explicit scheme, in which there is no need for the solution of simultaneous equations. Basically, the density of the fluid is related to the pressure through an artificial compressibility parameter, that needs to be properly computed from time step limitations [8, 9]. The new scheme has been tested for different fluid dynamic problems, and it proved to be efficient [8, 10]. However, its performance has not been compared yet to the semi-implicit version of the CBS. This work presents such a comparison for a number of benchmark problems, for which the solution is obtained using both versions of the CBS, for steady state and transient problems.

2 GOVERNING EQUATIONS

The governing Navier-Stokes equations for non-isothermal fluid can be written in their non-dimensional form, for forced convection problems:

Continuity equation:

$$\frac{\partial \rho}{\partial t} + \frac{\partial}{\partial x_i}(U_i) = 0 \tag{1}$$

where $U_i = \rho u_i$ is defined as mass flow fluxes, ρ is the density and u_i represents the velocity components. It should be noted that the transient density term in the continuity

equation can be replaced by the following relation under isentropic conditions:

$$\frac{\partial \rho}{\partial t} = \frac{1}{c^2}\frac{\partial p}{\partial t} \tag{2}$$

where c is speed of sound and p is the pressure. For many heat transfer applications the flow can be considered to be incompressible, and therefore $c^2 \to \infty$. However, in Artificial Compressibility (AC) schemes c is taken as an artificial parameter (β), of finite value, calculated from velocity and temperature fields [8].

Momentum equation:

$$\frac{\partial U_i}{\partial t} + \frac{\partial}{\partial x_j}(u_j U_i) = -\frac{\partial p}{\partial x_i} + \frac{\partial \tau_{ij}}{\partial x_j} \tag{3}$$

In the above equation τ_{ij} represents the deviatoric stress components, according to the following relation:

$$\tau_{ij} = \frac{1}{Re}\left(\frac{\partial u_j}{\partial x_j} + \frac{\partial u_j}{\partial x_i} - \frac{2}{3}\frac{\partial u_k}{\partial x_k}\delta_{ij}\right) \tag{4}$$

where δ_{ij} is the Kroneker delta and is equal to unity when $i = j$, while is equal to zero when $i \neq j$, and Re is the Reynolds number.

Energy equation:

$$\frac{\partial T}{\partial t} + \frac{\partial (T u_j)}{\partial x_j} - \frac{\partial}{\partial x_j}\left(\frac{1}{RePr}\frac{\partial T}{\partial x_j}\right) = 0 \tag{5}$$

with T fluid's temperature and Pr Prandtl number. The above non-dimensional equations are obtained employing the following scales and parameters:

$$u_i = \frac{u_i^*}{u_\infty};\ \rho = \frac{\rho}{\rho_\infty^*};\ x_i = \frac{x_i^*}{L};\ t = \frac{t^* u_\infty}{L};\ p = \frac{p^*}{\rho_\infty u_\infty}\ Re = \frac{u_\infty^* L}{\nu};\ Pr = \frac{\nu}{\alpha} \tag{6}$$

where u_∞ is the free stream velocity, ρ_∞ is the free stream density, L is characteristic length of the problem examined, ν is the kinematic viscosity of the fluid and α its thermal diffusivity. The asterisk is used here for dimensional quantities.

3 THE CHARACTERISTIC-BASED-SPLIT (CBS) SCHEME

The CBS scheme, based on the Galerkin spatial approximation, is presented in many papers [5, 7, 8, 10, 16] and is briefly discussed for the sake of completeness. The CBS procedure can be carried out using both semi-implicit and fully explicit formulation and can be implemented in two ways: in the first procedure the pressure term in the momentum equation is retained at its previous step value, while in the second procedure the pressure term is completely removed. The solutions of the continuity equation, momentum equation and energy equation is carried out in four steps. The following relations describe CBS procedure for problems dominated by forced convection.

Step 1: *intermediate momentum equation*

$$\begin{aligned}\Delta\widetilde{U}_i = \widetilde{U}_i - U_i^n &= \Delta t\left[-\frac{\partial}{\partial x_j}(u_j U_i)^n + \frac{\partial p^{n+\vartheta_2}}{\partial x_i} + \frac{\partial \tau_{ij}^n}{\partial x_j}\right] \\ &+\frac{\Delta t^2}{2}u_k\frac{\partial}{\partial x_k}\left(\frac{\partial}{\partial x_j}(U_i u_j)^n + \frac{\partial p^n}{\partial x_i}\right)\end{aligned} \tag{7}$$

where the pressure term is evaluated at a time $t^n + \vartheta_2\Delta t$ ($\vartheta_2 = 0$ for fully explicit scheme, $0 < \vartheta_2 \leq 1$ for semi-implicit or implicit form), according to the following relation:

$$\frac{\partial p^{n+\vartheta_2}}{\partial x_i} \equiv \vartheta_2\frac{\partial p^{n+1}}{\partial x_i} + (1-\vartheta_2)\frac{\partial p^n}{\partial x_i} \tag{8}$$

and $\Delta t = t^{n+1} - t^n$, while $\widetilde{U}_i$ indicate an intermediate value of the velocity components. The higher-order terms are obtained applying concept of discretization along characteristic curves.

Step 2: *density or pressure calculation*

$$\begin{aligned}\left(\frac{1}{\beta^2}\right)^n\left(p^{n+1} - p^n\right) &= -\Delta t\left[\vartheta_1\frac{\partial \widetilde{U}_i}{\partial x_i} + (1-\vartheta_1)\frac{\partial U_i^n}{\partial x_i}\right] \\ &+\Delta t^2\vartheta_1\left[\vartheta_2\frac{\partial^2 p^{n+1}}{\partial x_i \partial x_i} + (1-\vartheta_2)\frac{\partial^2 p^n}{\partial x_i \partial x_i}\right]\end{aligned} \tag{9}$$

where β, as mentioned before, is an artificial compressibility parameter that replaces then speed of sound c in continuity equation.

Step 3: *velocity correction*

$$U_i^{n+1} - \widetilde{U}_i = -\Delta t\frac{\partial p^{n+\vartheta_2}}{\partial x_i} + \frac{\Delta t^2}{2}u_k\frac{\partial}{\partial x_k}\left(\frac{\partial p^n}{\partial x_i}\right) \tag{10}$$

Step 4: *energy equation*

$$T^{n+1} - T^n = \Delta t\left[-\frac{\partial}{\partial x_j}(T u_j)^n + \frac{\partial}{\partial x_j}\left(\frac{1}{RePr}\frac{\partial T^n}{\partial x_j}\right)\right] + \frac{\Delta t^2}{2}u_k\frac{\partial}{\partial x_k}\left[\frac{\partial}{\partial x_j}(T u_j)^n\right] \tag{11}$$

The above equations are optimally solved using standard Galerkin finite element approximation [5]. The geometrical domain is discretized using finite elements in which the unknown quantity ϕ_i is approximated using the shape functions N_i as follows:

$$\phi = \sum_{i=1}^{m} N_i\phi_i \tag{12}$$

where m is the number of nodes in the element. All the unknown nodal quantities are therefore approximated as follows:

$$U_i = \mathbf{N_u U_i}; \qquad \widetilde{U}_i = \mathbf{N_u}\widetilde{\mathbf{U}}_\mathbf{i}; \qquad p_i = \mathbf{N_p p} \qquad T_i = \mathbf{N_t T} \tag{13}$$

The time-space-discrete set of algebraic equations can be obtained by weighting the residuals with the same shape functions used for the approximation. The resulting four steps of the CBS algorithm are [5, 8]:

Step 1: *intermediate momentum equation*

$$\begin{aligned}\int_\Omega \mathbf{N_u^T}\Delta\tilde{U}_i d\Omega &= \Delta t\left[-\int_\Omega \mathbf{N_u^T}\frac{\partial}{\partial x_j}(u_j U_i)d\Omega - \int_\Omega \frac{\partial \mathbf{N_u^T}}{\partial x_j}\tau_{ij}d\Omega\right]^n \\ &\quad -\frac{\Delta t^2}{2}\left[\int_\Omega \frac{\partial}{\partial x_j}\left(u_j \mathbf{N_u^T}\right)\frac{\partial}{\partial x_j}(u_j U_i)d\Omega\right]^n + \Delta t\left[\int_\Gamma \mathbf{N_u^T} t_i^* n_i d\Gamma\right]^n \end{aligned}\tag{14}$$

In the above equation the boundary integral term represents the part of traction that corresponds only to the deviatoric stress and n_i are the components of the outward normal to the boundaries of the domain.

Step 2: *density or pressure calculation*

$$\int_\Omega \mathbf{N_p^T}\left(\frac{1}{\beta^2}\right)^n \Delta p d\Omega = -\Delta t\int_\Omega \mathbf{N_p^T}\frac{\partial}{\partial x_i}\left(U_i^n + \vartheta_1\Delta\tilde{U}_i - \vartheta_1\Delta t\frac{\partial p^{n+\vartheta_2}}{\partial x_i}\right)d\Omega \tag{15}$$

where the right hand side is solved integrating by parts the pressure term and $\Delta\tilde{U}_i$ term.

Step 3: *velocity correction*

$$\begin{aligned}\int_\Omega \mathbf{N_u^T}\Delta U_i d\Omega &= \int_\Omega \mathbf{N_u^T}\Delta\tilde{U}_i d\Omega - \Delta t\left[\int_\Omega \frac{\partial \mathbf{N_u^T}}{\partial x_i}\left((1-\vartheta_2)p^n + \vartheta_2 p^{n+1}\right)d\Omega\right] \\ &\quad + \int_\Gamma \mathbf{N_u^T} t_i^{**} n_i d\Gamma\end{aligned}\tag{16}$$

in which the boundary integral includes the traction corresponding to the pressure term that was removed from the first step.

Step4: *Energy equation.*

$$\begin{aligned}\int_\Omega \mathbf{N_t^T}\Delta T d\Omega &= -\Delta t\left[\int_\Omega \mathbf{N_t^T}\left(\frac{\partial T u_j}{\partial x_j}\right)d\Omega + \frac{1}{RePr}\int_\Omega \mathbf{N_t^T}\frac{\partial T}{\partial x_j}d\Omega\right]^n \\ &\quad -\frac{\Delta t^2}{2}\left[\int_\Omega \frac{\partial}{\partial x_k}(\mathbf{N_t^T}u_k)\left(\frac{\partial}{\partial x_j}(Tu_j)\right)d\Omega\right]^n \\ &\quad +\Delta t\left[\int_\Gamma \mathbf{N_t^T} t' n_i d\Gamma\right]^n + \frac{\Delta t^2}{2}\left[\int_\Gamma \mathbf{N_t^T} t'' n_i d\Gamma\right]^n\end{aligned}\tag{17}$$

In this equation all the second order terms are integrated by parts, and this brings in the formulation the boundary integral terms. The solution of the problem, as mentioned above, is obtained using the Artificial Compressibility (AC) scheme (β parameter) [8]. The actual compressible wave speed c in the continuity equation involves, especially for the fully explicit scheme, severe time step restrictions. As β is a local parameter, the time step is also calculated as local parameter in the both semi-implicit and fully explicit scheme and is related to β parameter by the following relations [8].

$$\beta = max(\varepsilon, v_{conv}, v_{diff}) \tag{18}$$

where ε is a constant taken as 0.5, v_{conv} is the convective velocity and v_{diff} is the diffusive velocity.

$$v_{conv} = \sqrt{u_i u_i} \tag{19}$$

$$v_{diff} = \frac{2}{hRe} \tag{20}$$

with h minimum local element size [8]. The local time step is assumed as the minimum between the convective local time step and diffusive local time step using the following:

$$\Delta t = min(\Delta t_{conv}, \Delta t_{diff}) \tag{21}$$

$$\Delta t_{conv} = \frac{h}{u_{conv} + \beta} \tag{22}$$

$$\Delta t_{diff} = \frac{h^2 Re}{2} \tag{23}$$

4 NUMERICAL RESULTS

In this work four benchmark examples are considered in order to compare the fully explicit and semi-implicit versions of the scheme. The results obtained are compared with other numerical and experimental data available in literature.

4.1 Lid-driven cavity

The first problem considered is the lid-driven cavity. The square cavity has a no-slip velocity on the bottom and side walls, while the top-lid moves with a given horizontal velocity, as shown un Figure 1. In order to explore the performance of the scheme, the problem is solved using two different finite element meshes. Figure 1 presents these meshes: the first with 1251 nodes and 2888 elements, and the second with 5515 nodes and 10596 elements.

The mesh 1 is used to solve convective flow with Reynolds number up to value of 5000.

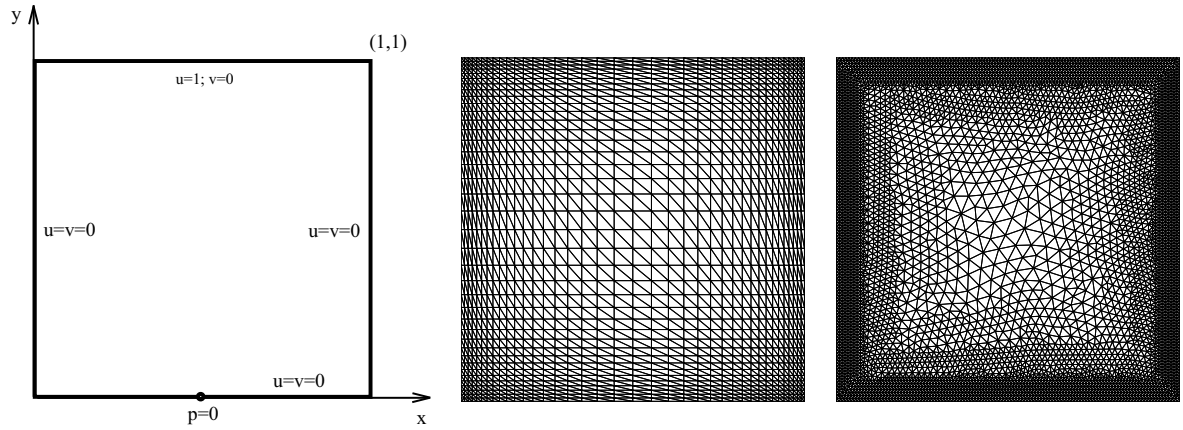

Figure 1: Lid-driven cavity problem: (a) computational domain and boundary conditions; (b) mesh 1, 1251 nodes and 2888 elements; (c) mesh 2, 5515 nodes and 10596 elements

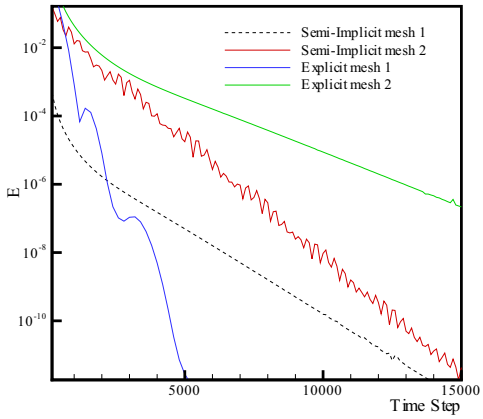

Figure 2: Convergence history for both semi-implicit and fully explicit scheme.

The convergence history plotted in Figure 2 is evaluated in terms of the norm of the difference between the velocity calculated at two consecutive time steps, normalized with respect to the first time step. This figure also shows the mesh influence on convergence velocity for Reynolds number of 100. It's important to note that the fully explicit scheme shows a faster rate of convergence.

In Figure 3, pressure, horizontal velocity and vertical velocity contours are presented for the explicit and semi-implicit schemes at two different Reynolds numbers, 400 and 5000. These results were obtained using the coarser mesh, and show a slight difference of the two solutions at higher Reynolds numbers. In particular, the semi-implicit scheme presents smoother results near the bottom right and the top left corners.

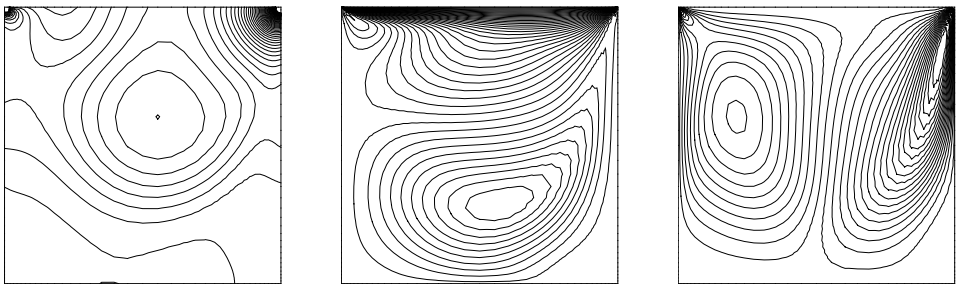

$Re = 400$, explicit.

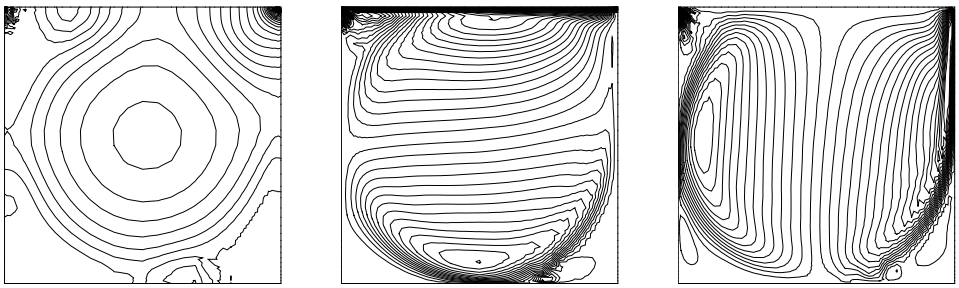

$Re = 5000$, explicit.

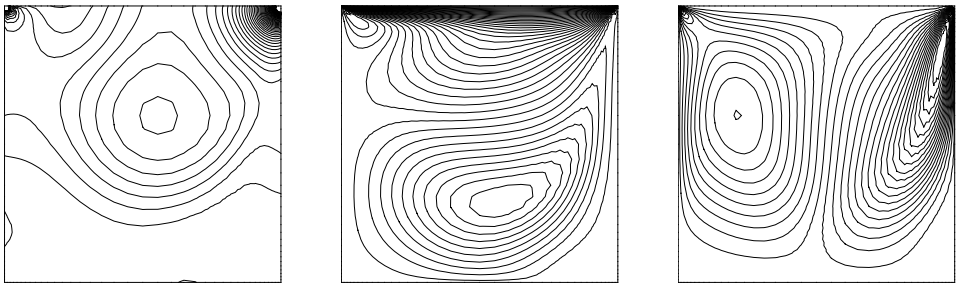

$Re = 400$, semi-implicit.

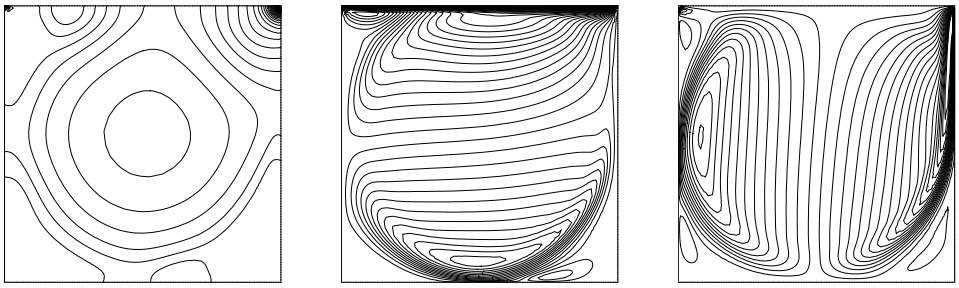

$Re = 5000$, semi-implicit.

Figure 3: Lid-driven cavity. From left to right: pressure, horizontal velocity, and vertical velocity contours for the lid driven cavity.

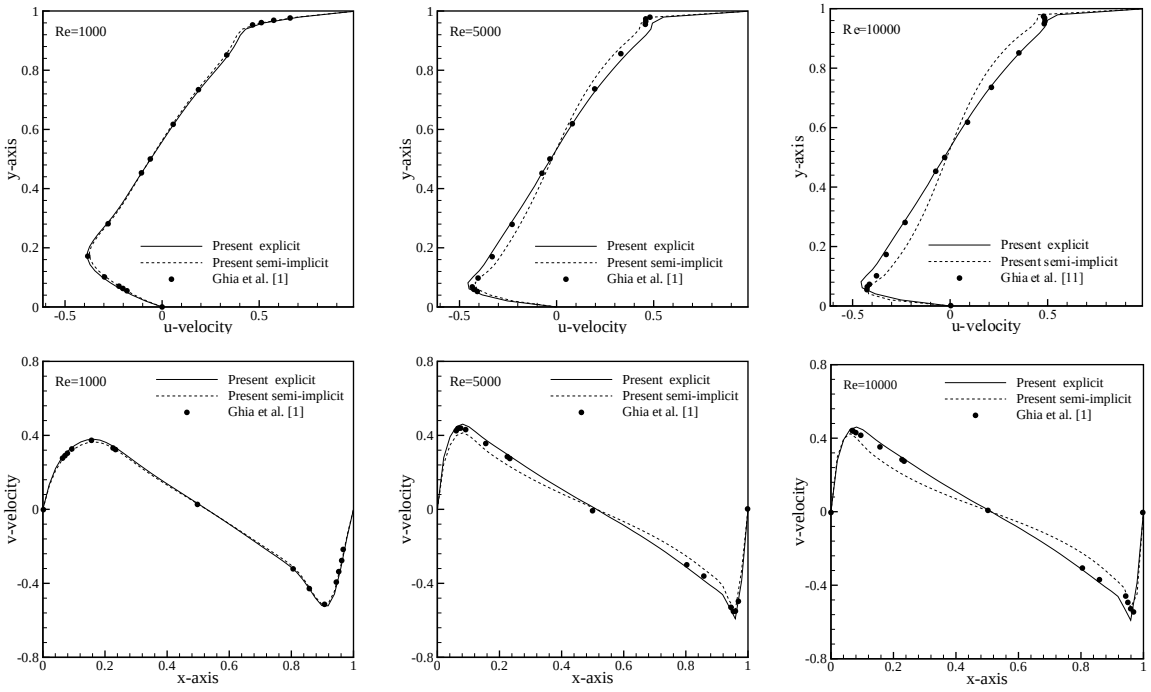

Figure 4: horizontal and vertical velocity distributions at mid-height along x- and y-direction for different Reynolds numbers: $Re = 1000$, $Re = 5000$, $Re = 10000$.

Figure 4 shows a comparison of the present results with other numerical data obtained by Ghia *et al.* [11] using a very fine mesh. Both the horizontal and vertical velocities, respectively at mid vertical and horizontal sections, are shown for Reynolds numbers of 1000, 5000 and 10000. It can be noticed that the two version of the scheme produce different results, and at higher Re, the solution obtained with the explicit code agrees better with Ghia's results.

4.2 Backward facing step

The backward facing step is another test case commonly employed to validate a numerical solution of incompressible Navier-Stokes equations. The configuration considered in this work is the one for which experimental data are available in literature [12]. The computational domain with the boundary conditions are presented in Figure 5.(a). In particular, the velocity at the inlet is approximated with the profile that was obtained in the experiments [12]. Furthermore, the measurement section in the experiments was placed 1.3 step heights upstream the step. This was also taken into account in the present calculations. However, the distance between the inlet section and the step is usually assumed to be 4 step heights in all the other numerical simulations [13, 14, 15, 16]. For the heat transfer results, this configuration, with a fully developed parabolic profile was

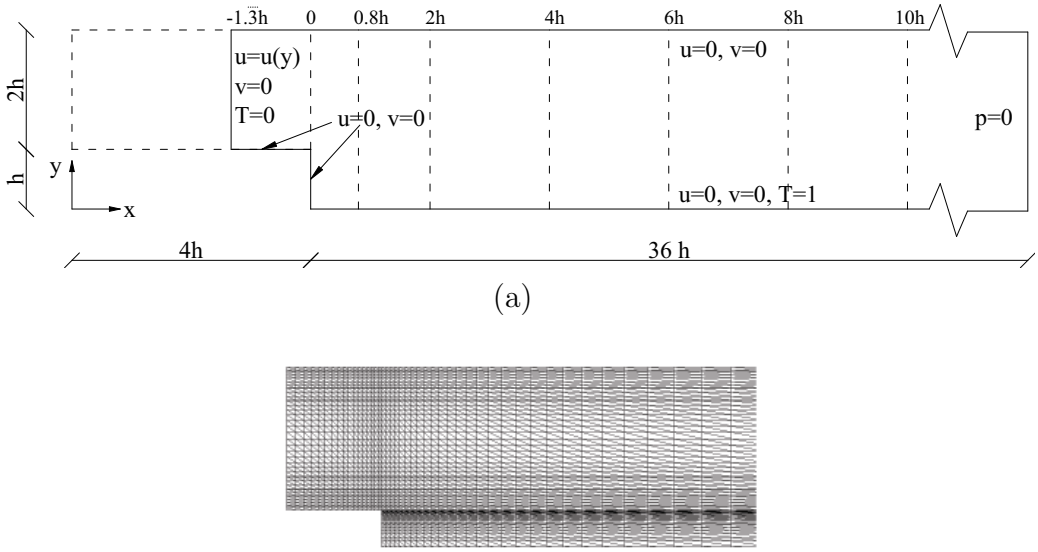

(a)

(b)

Figure 5: Backward facing step: (a) computational domain and boundary conditions; (b) particular of the mesh.

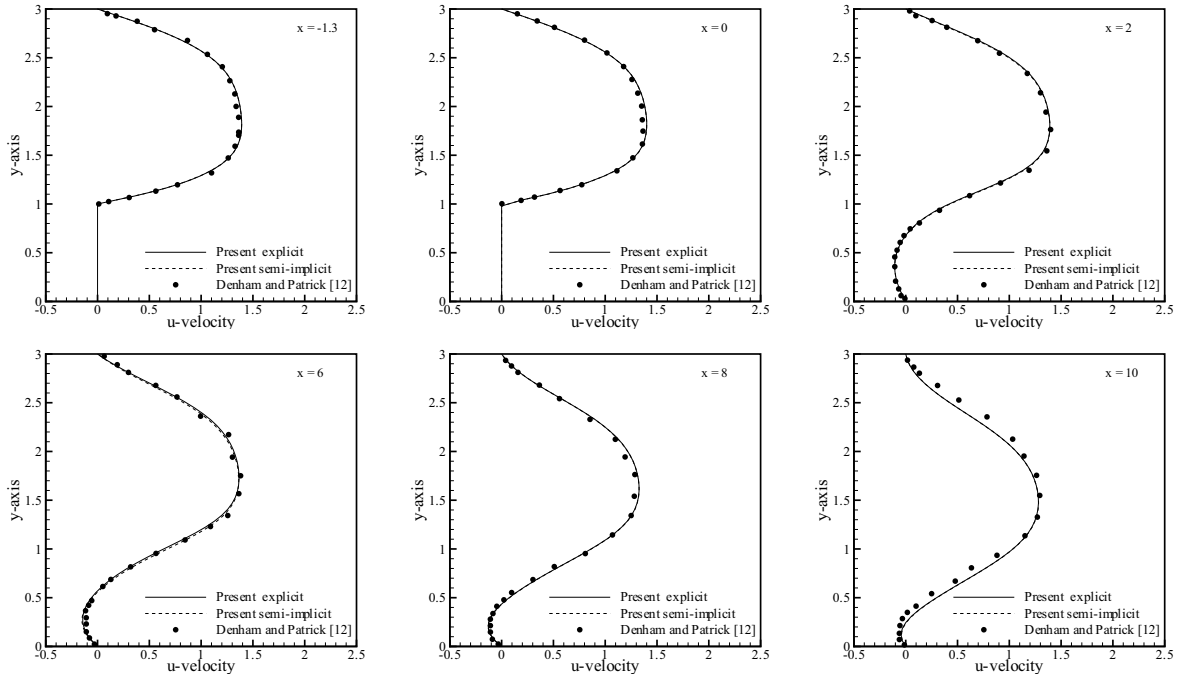

Figure 6: Flow over a backward facing step. Horizontal velocity distribution.

also considered (Figure 5.(a)). All the walls have non-slip boundary conditions for the velocity . As regards the thermal boundary conditions (Figure 5), the bottom wall has a temperature equal to one, while the inlet temperature is equal to zero. All the other wall are considered to be adiabatic. Figure 5.(b) shows a detail of the mesh used, composed of 4183 nodes and 8092 triangular elements.

Figure 6 shows the horizontal velocity distribution on different vertical sections along the channel (Figure 5). The velocity profiles obtained with both versions of the scheme are practically the same, and show an excellent agreement with the experimental data. Figure 7 shows the pressure, horizontal velocity and temperature contours obtained with the two versions of the scheme. In this case it can be seen that the contours are the same also from a qualitative point of view.

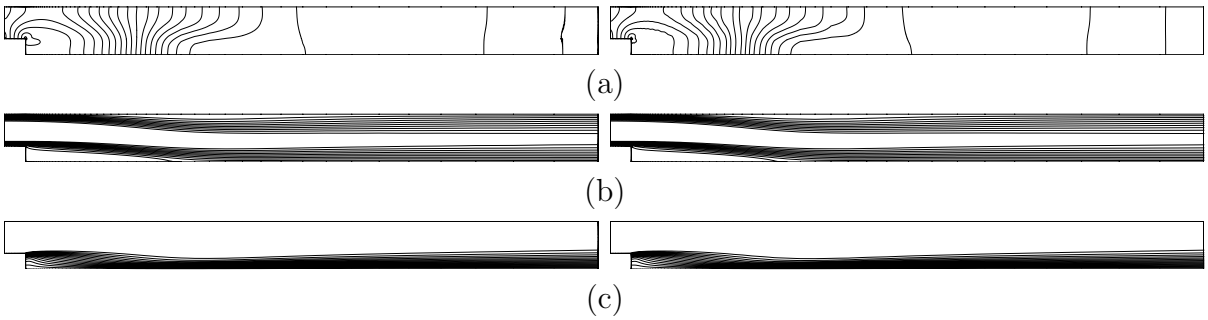

Figure 7: Backward facing step. Fields obtained for Re=299 using fully explicit scheme (left) and semi-implicit scheme (right). a) pressure distribution; b)u-velocity distribution; c) temperature distribution.

In Figure 8 the convergence history is presented for the horizontal velocity, obtained for a Reynolds number of 100. Form this figure it may seem that the semi-implicit scheme is faster than fully explicit. However, due to the computational time needed for matrix matrix inversion, the semi-implicit took more computational time to converge than the fully explicit formulation.

The next plot (Figure 9) presents the value of the reattachment length, beyond the step, which is an relevant fluid dynamic parameter for this problem. The results obtained show that both codes give the same results and these are in good agreement with the experiments available from the literature [12, 13]. In terms of heat transfer quantities the temperature profile at two different vertical sections placed downstream the step are presented in Figure 10 for the case of fully developed inlet profile with Re=233. The profiles are the same for both the explicit and semi-implicit codes, and they show a very good agreement with the experimental data available from literature [14].

4.3 Natural convection in a square cavity

In this case, the flow is driven by the buoyancy forces due to the temperature differences in the fluid. Therefore, including these forces in the momentum equation, and using a

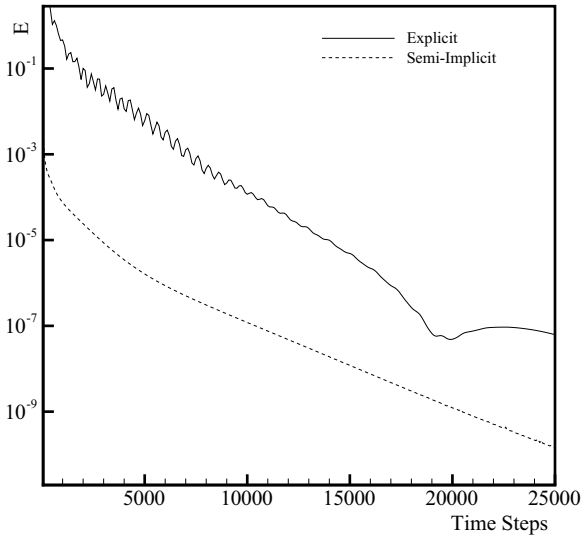

Figure 8: Convergence history for the horizontal velocity at Reynolds number 100 value.

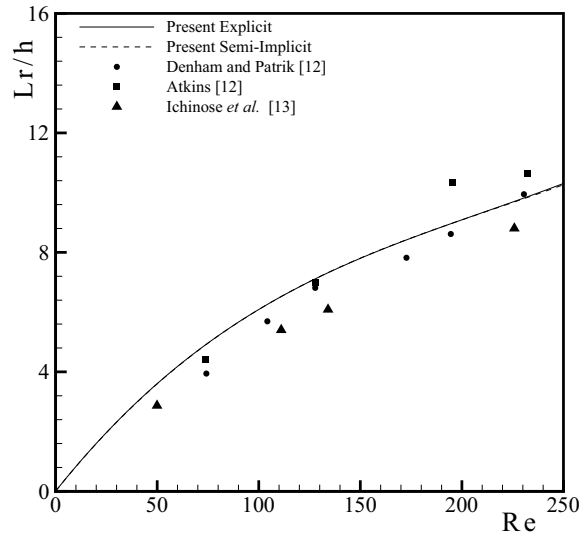

Figure 9: Backward facing step: reattachment length at different Reynolds numbers

different non-dimensional quantities, the equation becomes:

Momentum equation:

$$\frac{\partial U_i}{\partial t} + \frac{\partial}{\partial x_j}(u_j U_i) = -\frac{\partial p}{\partial x_i} + \frac{\partial \tau_{ij}}{\partial x_j} + \gamma_i RaPrT \tag{24}$$

where γ_i are the components of the unit vector in the vertical direction, and Ra represents

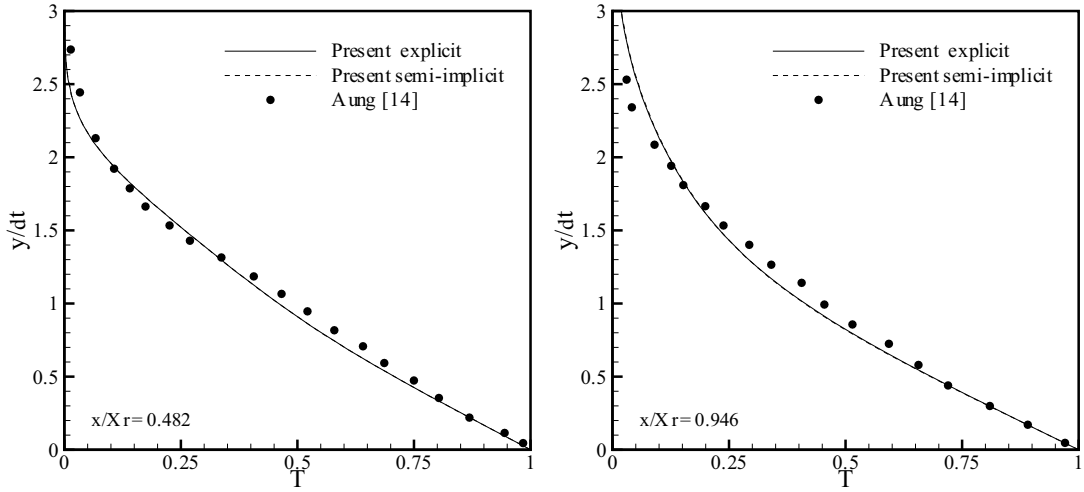

Figure 10: Backward facing step: Temperature profiles at two different sections downstream the step (Re=233).

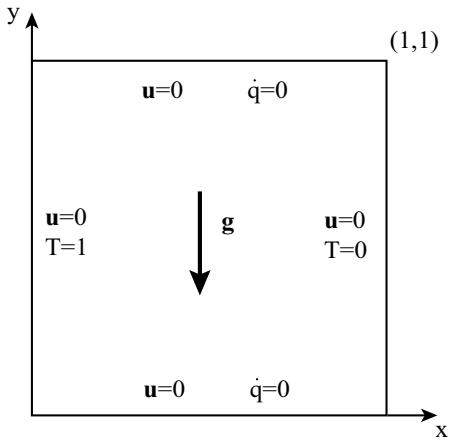

Figure 11: Natural convection in a square cavity: computational domain and boundary conditions.

the Rayleigh number:

$$Ra = \frac{g\beta(T_h - T_c)L^3}{\nu\alpha} \tag{25}$$

with g gravitational acceleration, β coefficient of thermal expansion, and T_h, T_c respectively the highest and lowest temperatures in the cavity. Furthermore, the deviatoric stress is multiplied by the Prandtl number, and the diffusion terms in the energy equation appears with a unit coefficient. For further details on the non-dimensional equations

for natural convection problems the reader should refer to the literature [16].

Figure 11 presents the problem definition. Both the horizontal walls are thermally insulated, while the vertical sides are kept at different temperatures. For all walls no-slip velocity condition are assumed. The mesh used for this case is the same coarse one used for the lid-driven cavity problem (Figure 1).

Figures 12 and 13 show the temperature contours and streamlines obtained with the two schemes at different Rayleigh numbers. The agreement between the two solutions obtained are practically the same. This is confirmed by the calculation of the Nusselt number on the hot wall, presented in Figure 14. The solutions obtained are symmetric with respect to the center of the cavity, and compare very well with other numerical data as it was shown in previous work [16]. From the computational point of view, the semi-implicit version of the code was much slower than the explicit.

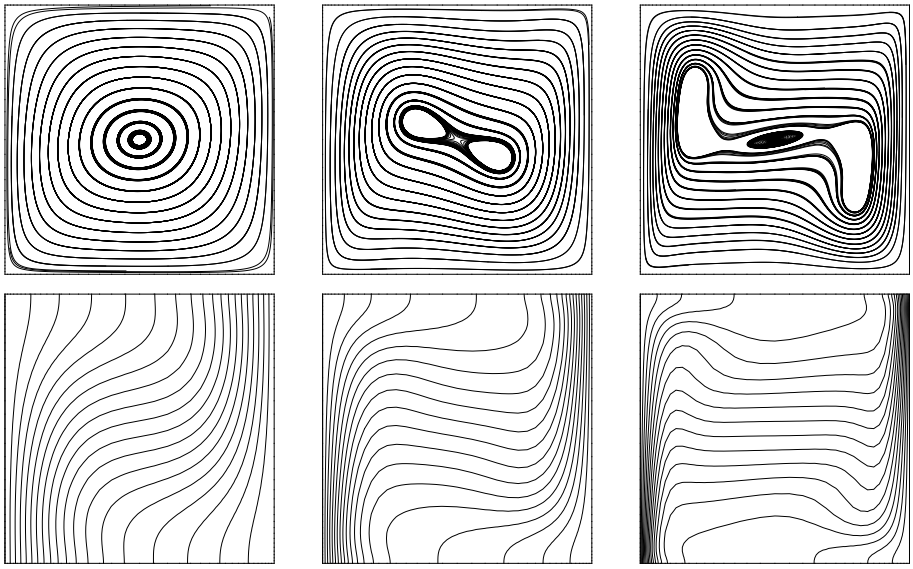

Figure 12: Natural convection in a square cavity. Streamlines (top) and isotherms (bottom) obtained with the fully explicit scheme.

4.4 Transient flow over a circular cylinder

The transient test case considered is the non-isothermal flow over a circular cylinder. The time stepping scheme provides the transient solution only for the semi-implicit version of the CBS. A detailed description of the procedure used to obtain transient solutions from the explicit version of the code is presented elsewhere [8, 10].

The problem definition is shown in Figure 15.(a) with the boundary conditions assumed: uniform flow and temperature at the inlet, non-slip velocity and uniform tem-

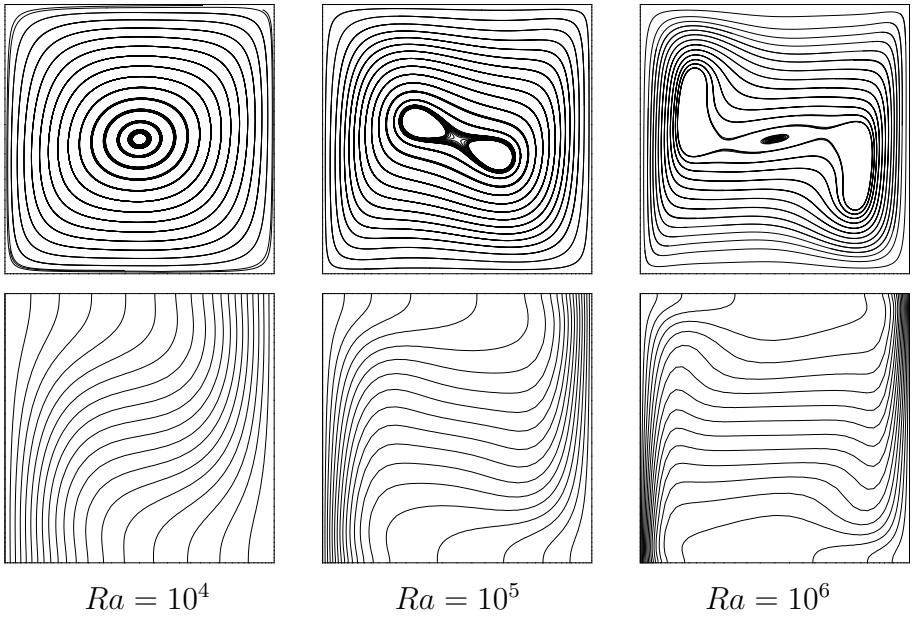

Figure 13: Natural convection in a square cavity. Streamlines (top) and isotherms (bottom) obtained with the semi-implicit scheme.

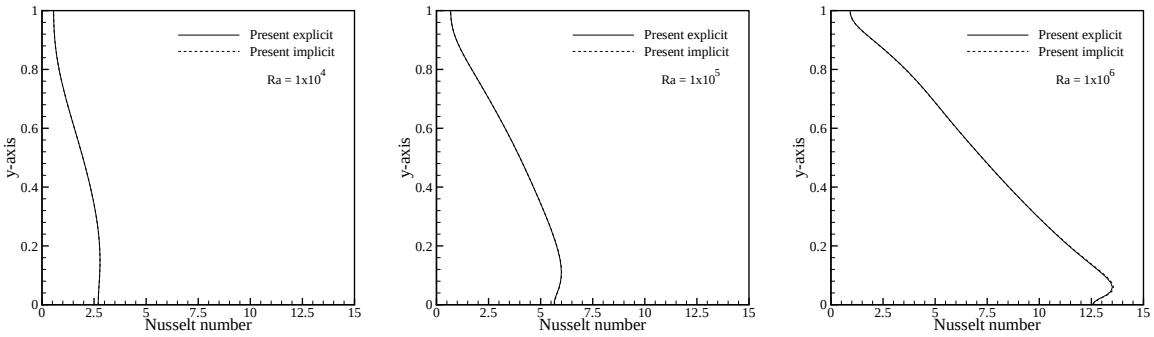

Figure 14: Natural convection in a square cavity: local Nusselt number distribution along hot wall.

perature (T=1) on the cylinder's surface, slip flow and adiabatic horizontal walls. The cylinder is placed at the center between to the two horizontal walls of the channel considered, at a distance from the inlet section equal to four times the cylinder's diameter. The whole computational domain is $16D$ long. The mesh used for this problem is constituted by 13990 triangular elements and 7129 nodes (Figure 15.(b)).

In the solution of the transient problem the two versions of the scheme showed the main differences. In fact, the results presented in Figures 16 and 17, where the explicit and implicit horizontal velocity and isotherms are presented, show that the beginning of the

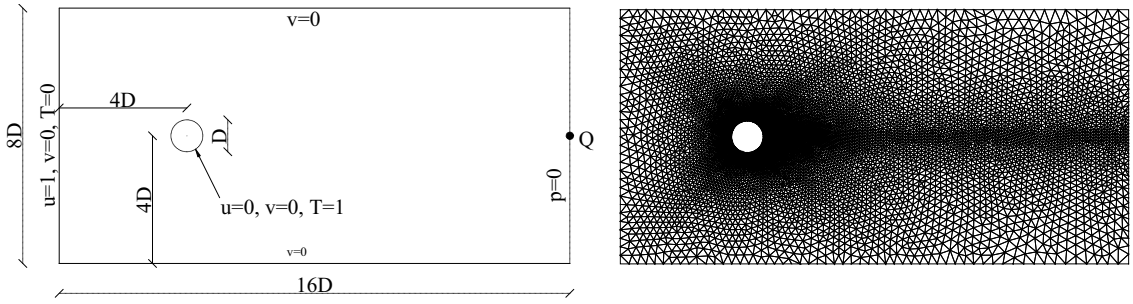

(a) (b)

Figure 15: Vortex shedding: (a) computational domain and boundary conditions; (b) mesh: 7129 nodes and 13990 elements.

transient vortices behind the cylinder start earlier with the explicit code. Furthermore, for a given time, the oscillations behind the cylinder are more pronounced in the semi-implicit solution. Figure 18, which presents the variation of the vertical velocity component with time, shows that the amplitude and frequency of the velocity oscillations are slightly different in the two solutions obtained. In particular, from the comparison with the data available from literature, the semi-implicit solution has higher amplitude, which better approximates the data of de Sampaio *et.al* [15], while the frequency of the oscillations presented in [15] is better approximated by the explicit code. At the moment, this results can be attributed only to the different order of approximation of the temporal derivatives in the two formulations. However, further study is needed in order to fully explain the differences obtained.

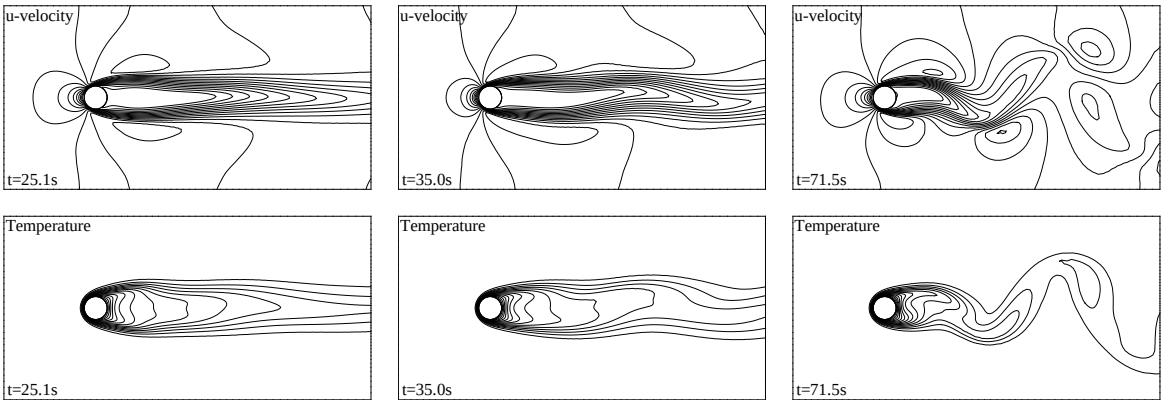

Figure 16: Vortex shedding behind a circular cylinder: horizontal velocity and temperature contours obtained with fully explicit scheme.

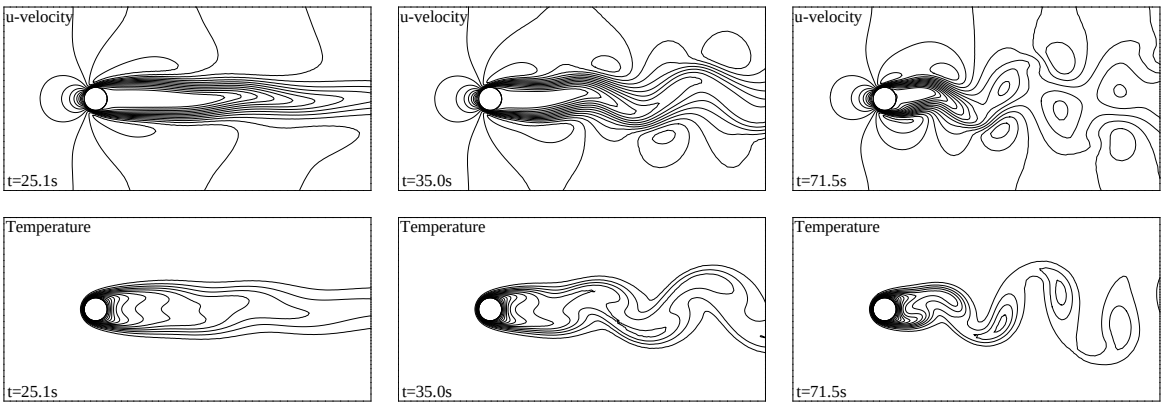

Figure 17: Vortex shedding behind a circular cylinder: horizontal velocity and temperature contours obtained with semi-implicit scheme.

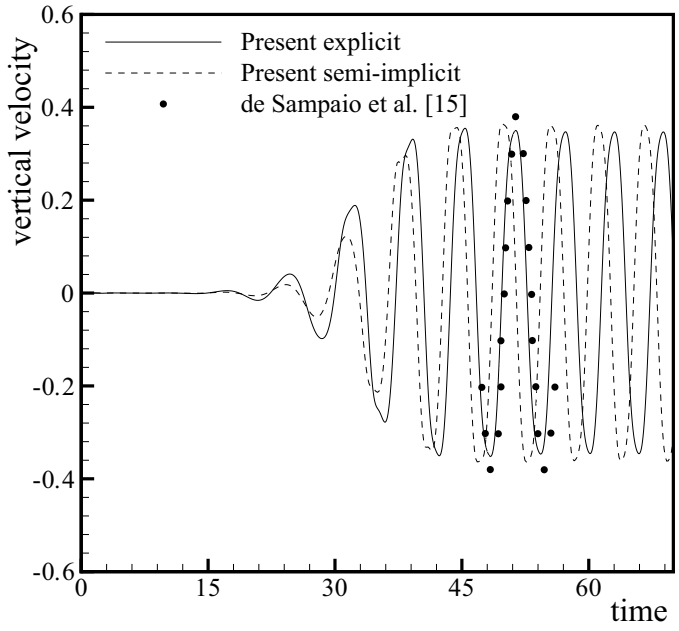

Figure 18: Vortex shedding: vertical velocity at the mid-height exit point (Q in Figure 15).

5 CONCLUSIONS

The paper has compared two versions of the CBS scheme for the solution of incompressible flows with heat transfer. In particular, the classic semi-implicit version of the scheme is compared to the new fully explicit formulation. The main results of the comparison carried out can be summarized as follow:

- the two formulations showed very good performances in the solution of all the benchmark problems solved.
- Slight differences were noticed in the solutions of velocity field in the lid driven cavity problem.
- All the other steady state solutions obtained with the two formulations where practically the same, especially those for natural convection problems.
- The solution of the transient problem (vortex shedding behind a circular cylinder) has shown a difference between the two solutions obtained. This is probably due to the time approximations used for the two schemes, but further study is needed to confirm it.
- The fully explicit version of the code needs less computational time than the semi-implicit and represents therefore a important improvement of the CBS scheme.

The CBS scheme is a very general and reliable algorithm for the solution of fluid dynamic and heat transfer problems. The latest formulation developed, being fully explicit is also very fast. The algorithm should definitely be implemented in commercial CFD codes.

REFERENCES

[1] G. Comini, and S. Del Giudice. Finite element solution of incompressible Navier-Stokes equations. *Numerical Heat Transfer: Part A*, **5**, 463–478, 1972.

[2] J.T. Oden, and L.C. Wellford. Analysis of flow of viscous fluids by finite element method. *AIAA Journal*, **10**, 1590–1599, 1972.

[3] C. Taylor, and P. Hood. A numerical solution of the Navier-Stokes equations using the finite element technique. *Computer and Fluids*, **1**, 73–100, 1973.

[4] G.E. Schneider, G.D. Raithby, and M.M. Yovanovich. Finite element analysis of incompressible fluid flow incorporating equal order pressure and velocity interpolation. *Numerical Methods in Laminar and Turbolent Flow*. Pentech, 1978.

[5] O.C. Zienkiewicz and R.L. Taylor. *The Finite Element Method, vol.3, Fluid Dynamics*. Butterworth and Heinemannm, 2000.

[6] D.B. Spalding. A novel finite difference furmulation for differential equations involving both first and second order derivatives. *International Journal for Numerical Methods in Engineering*, **4**, 551–559, 1972.

[7] O.C. Zienkiewicz, and R. Codina. A general algorithm for compressible and incompressible flow, Part I. The split characteristic based scheme. *International Journal for Numerical Methods in Fluids*, **20**, 869-885, 1995.

[8] P. Nithiarasu. An efficient artificial compressibility (AC) scheme based on split (CBS) method for incompressible flows. *International Journal for Numerical Methods in Engineering*, **56**, 1815–1845, 2003.

[9] A.G. Malan, R.W. Lewis, and P. Nithiarasu. An improved unsteady, unsctructured, artificial compressibility, finite volume scheme for viscous incompressible flows: part I. Theory and implementation. *International Journal for Numerical Methods in Engineering*, **54**, 695–714, 2002.

[10] P. Nithiarasu, J.S. Mathur, N.P. Weatherill, and K. Morgan. Three dimensional incompressible flow calculations using the Characteristic Based Split (CBS) scheme. *International Journal for Numerical Methods in Fluids*, **44**, 1207-1229, 2004.

[11] U. Ghia, K.N. Ghia and C.T. Shin. High-Re solutions for incompressible flow using the NavierStokes equations and multigrid method. *Journal of Computational Physics*, **48**, 387-411, 1982.

[12] M.K. Denham, M.A. Patrik. Laminar flow over a downstream-facing in a two-dimensional flow channel. *Transactions of the Institution of Chemical Engineers*, **52**, 361-367,1974.

[13] K. Ichinose, H. Tokunaga, N. Satofuka. Numerical simulation of two-dimesnional backward-facing step flows. *Transactions of JSME B*, **57-543** 3715–3721, 1991.

[14] W. Aung. An experimental study of laminar heat transfer downstream of backsteps. *Journal of Heat Transfer*, **105**, 823–829, 1983.

[15] P.A.B. de Sampaio, P.R.M. Lyra, K. Morgan, and N.P. Weatherill. PetrovGalerkin solutions of the incompressible NavierStokes equations in primitive variables with adaptive remeshing. *Computer Methods in Applied Mechanics and Engineering*, **106**, 143-178, 1993.

[16] N. Massarotti, P. Nithiarasu, and O.C. Zienkiewicz. Characteristic-Based-Split (CBS) algorithm for incompressible flow problems with heat transfer. *International Journal for Numerical Methods in Heat and Fluid Flow*, **8**, 969-990, 1998.